

A unified understanding of minimum lattice thermal conductivity

Yi Xia,^{1,*} Dale Gaines II,² Jiangang He,³ Koushik Pal,² Mercuri G. Kanatzidis,⁴ Vidvuds Ozoliņš,^{5,†} and Chris Wolverton^{2,‡}

¹*Department of Mechanical and Materials Engineering, Portland State University, Portland, OR 97201, USA*

²*Department of Materials Science and Engineering, Northwestern University, Evanston, IL 60208, USA*

³*School of Mathematics and Physics, University of Science and Technology Beijing, Beijing 100083, China*

⁴*Department of Chemistry, Northwestern University, Evanston, IL 60208, United States, Materials Science Division, Argonne National Laboratory, Argonne, IL 60439, United States*

⁵*Department of Applied Physics, Yale University, New Haven, CT 06511, USA, Energy Sciences Institute, Yale University, West Haven, CT 06516, USA*

(Dated: June 22, 2023)

We propose a first-principles model of minimum lattice thermal conductivity (κ_L^{\min}) based on a unified theoretical treatment of thermal transport in crystals and glasses. We apply this model to thousands of inorganic compounds and discover a universal behavior of κ_L^{\min} in crystals in the high-temperature limit: the isotropically averaged κ_L^{\min} is independent of structural complexity and bounded within a range from ~ 0.1 to ~ 2.6 W/[m·K], in striking contrast to the conventional phonon gas model which predicts no lower bound. We unveil the underlying physics by showing that for a given parent compound κ_L^{\min} is bounded from below by a value that is approximately insensitive to disorder, but the relative importance of different heat transport channels (phonon gas versus diffuson) depends strongly on the degree of disorder. Moreover, we propose that the diffuson-dominated κ_L^{\min} in complex and disordered compounds might be effectively approximated by the phonon gas model for an ordered compound by averaging out disorder and applying phonon unfolding. With these insights, we further bridge the knowledge gap between our model and the well-known Cahill-Watson-Pohl (CWP) model, rationalizing the successes and limitations of the CWP model in the absence of heat transfer mediated by diffusons. Finally, we construct graph network and random forest machine learning models to extend our predictions to all compounds within the Inorganic Crystal Structure Database (ICSD), which were validated against thermoelectric materials possessing experimentally measured ultralow κ_L . Our work offers a unified understanding of κ_L^{\min} , which can guide the rational engineering of materials to achieve κ_L^{\min} .

I. INTRODUCTION

Knowing the lower limit to the lattice thermal conductivity of crystals is of fundamental interest and technological importance, particularly relevant to thermal energy conversion and management applications [1]. The minimum lattice thermal conductivity (κ_L^{\min}), a concept first proposed by Slack [2], sets the upper limit of thermoelectric conversion efficiency for a given electronic transport profile [3–6] and provides the maximum thermal insulation for a substrate used in thermal barrier coatings [7, 8]. The fundamental physics of heat transport in crystals at the lower limit of thermal conductivity continues to be an active research topic [2, 7, 9, 10].

Motivated by the observation that the experimentally accessible κ_L^{\min} is often found in amorphous solids, the initial attempts to understand κ_L^{\min} [11, 12] relied on a model proposed by Einstein [13], who assumed that the mechanism of heat transport in crystals was a random walk of the thermal energy between neighboring atoms vibrating with random phases. Einstein’s random walk model was later generalized by Cahill, Watson, and

Pohl [9] (referred to as the CWP model) to incorporate the Debye model of vibrations by adopting a wavelength-dependent mean free path (MFP). An earlier approach by Slack [2] as well as the more recent study by Clarke [7] also assumed that phonons are the dominant heat carriers, but used different assumptions about the phonon MFP. The CWP, Slack, and Clarke theories of κ_L^{\min} are all based on the conventional phonon gas model (PGM) and the Boltzmann gas kinetic equation [14], where the primary heat carriers are propagating phonons [10]. On the other hand, recognizing the potential failure of the PGM in the disordered regime, Allen and Feldman [15, 16] developed the diffuson theory of heat transport in disordered solids. The Allen-Feldman theory is based on Kubo-Greenwood formula in the harmonic approximation and the primary heat carriers are diffusons, which are described by the off-diagonal terms of the heat flux operator. Recently, a phenomenological κ_L^{\min} model was developed by Agne, Hanus, and Snyder [10] based on the diffuson theory, aiming to resolve the overestimation of κ_L^{\min} from the CWP model in comparison to experiments.

Despite significant advances, a comprehensive understanding of κ_L^{\min} is still elusive. A crucial yet missing piece of the puzzle is a first-principles-based theory that accurately describes κ_L^{\min} over the whole spectrum of materials between the prototypical classes of simple crystals and disordered amorphous solids. The development of such an advanced model would shed light on crucial open

* yxia@pdx.edu

† vidvuds.ozolins@yale.edu

‡ c-wolverton@northwestern.edu

questions. For instance, the heat transfer pathways mediated by localized diffusons and propagating phonons are often classified into independent channels [17–21]. Is there a unified physical picture of the two different kinds of heat carriers when approaching κ_L^{\min} ? Why does the CWP model work remarkably well for solids with strong disorder, despite retaining the PGM nature and neglecting all optical phonons [9, 11, 12]? There are recent experimental discoveries of crystalline compounds with ultralow and glass-like lattice thermal conductivity κ_L that resembles κ_L^{\min} [22–26]. What is the general behavior of κ_L^{\min} in crystals, i.e., how does it vary with structural complexity and atomic composition? Ultimately, is there a physical lower or upper bound to κ_L^{\min} ?

II. RESULTS AND DISCUSSIONS

Recent theoretical advances towards a unified theory of thermal transport in crystals and glasses have enabled a consistent treatment of different heat carriers such as propagating phonons and localized diffusons [28, 29]. Herein, we construct a κ_L^{\min} model based on the unified theory of Simoncelli, Marzari, and Mauri [28, 30] by adopting the approximation that each phonon mode’s lifetime is equal to one half of its vibrational period, $\tau_{\mathbf{q}}^s = \pi/\omega_{\mathbf{q}}^s$. This assumption follows the original proposal by Einstein [13] which was later adopted by the CWP model [9]. We choose not to use the minimum MFP criteria (e.g., by assuming that MFP is equal to the smallest atomic spacing) because for optical phonon modes with vanishing group velocities it will lead to infinite phonon lifetimes, which is unphysical and tends to diminish their off-diagonal contribution to thermal conductivity (see below). Using the formula for thermal conductivity from Ref. [28], we arrive at the following expression:

$$\kappa_L^{\min} = \frac{\pi \hbar^2}{k_B T^2 V N_{\mathbf{q}}} \sum_{\mathbf{q}} \sum_{s, s'} \frac{(\omega_{\mathbf{q}}^s + \omega_{\mathbf{q}}^{s'})^2}{2} \mathbf{v}_{\mathbf{q}}^{s, s'} \otimes \mathbf{v}_{\mathbf{q}}^{s', s} \cdot \frac{\omega_{\mathbf{q}}^s n_{\mathbf{q}}^s (n_{\mathbf{q}}^s + 1) + \omega_{\mathbf{q}}^{s'} n_{\mathbf{q}}^{s'} (n_{\mathbf{q}}^{s'} + 1)}{4\pi^2 (\omega_{\mathbf{q}}^{s'} - \omega_{\mathbf{q}}^s)^2 + (\omega_{\mathbf{q}}^s + \omega_{\mathbf{q}}^{s'})^2} \quad (1)$$

where \hbar , k_B , T , V , $N_{\mathbf{q}}$ are, respectively, the reduced Planck constant, the Boltzmann constant, the absolute temperature, the volume of the unit cell, and the total number of sampled phonon wave vectors. Phonon modes are denoted by the wave vector \mathbf{q} and mode index s . The key quantities entering Eq.[1] are phonon mode-resolved frequencies $\omega_{\mathbf{q}}^s$, population numbers $n_{\mathbf{q}}^s$, and the generalized group velocity tensors $\mathbf{v}_{\mathbf{q}}^{s, s'}$, with the latter calculated as [16, 28]

$$\mathbf{v}_{\mathbf{q}}^{s, s'} = \frac{i}{\omega_{\mathbf{q}}^s + \omega_{\mathbf{q}}^{s'}} \sum_{\alpha, \beta} \sum_{m, p, q} e_{\mathbf{q}}^s(\alpha, p) D_{\beta\alpha}^{pq}(0, m) \times (\mathbf{R}_m + \mathbf{R}_{pq}) e^{i\mathbf{q}\cdot\mathbf{R}_m} e_{\mathbf{q}}^{s'}(\beta, q). \quad (2)$$

Here, e , D , and \mathbf{R} denote the polarization vector, the dynamical matrix, and the lattice vector, respectively. α/β , m , and p/q are indices labeling the Cartesian coordinate, the unit cell, and the atoms within the unit cell.

Physically, we can further decompose κ_L^{\min} into two parts: the diagonal part with $s = s'$, which corresponds to the PGM, denoted as PGM- κ_L^{\min} , and the off-diagonal part, which accounts for the diffuson channel, denoted as OD- κ_L^{\min} . The total κ_L^{\min} will be referred to as PGM+OD- κ_L^{\min} . Immediately, we see that the evaluation of Eq.[1] only requires the knowledge of the harmonic phonon dispersion, making it amenable to large-scale DFT calculations. We applied Eq.[1] to a selected set of 2576 inorganic compounds, taking advantage of the tabulated harmonic force constants within the phonon database (phononDB) generated by Togo *et al.* [31, 32] using crystalline structures from the Materials Project (MP) [33–35].

Temperature enters Eq. (1) both explicitly in the prefactor and implicitly via the phonon occupation numbers $n_{\mathbf{q}}^s$. Because κ_L^{\min} increases monotonically with increasing temperature up to the Debye temperature as a result of enhanced heat capacity [9], and κ_L^{\min} in crystals is usually approached at high temperatures, we focus on exploring the high-temperature regime. We performed calculations at $T = 300, 600, \text{ and } 900$ K. We find that κ_L^{\min} of most compounds calculated at 600 K exhibit considerable increment over those calculated at 300 K, whereas κ_L^{\min} varies by less than 5% between $T = 600$ and 900 K for approximately 95% of the studied compounds, with the largest decrease being only 14%. Considering the larger availability of experimental measurements of κ_L at 600 K than 900 K, we will focus on the $T = 600$ K results in the following discussion. For anisotropic crystals, the components of κ_L^{\min} are further averaged along the three principle crystallographic axes. We refer the readers to the Methods section for a more detailed discussion of the structure types, chemical compositions, and criteria for numerically converging κ_L^{\min} .

The calculated values of PGM- κ_L^{\min} , OD- κ_L^{\min} , and PGM+OD- κ_L^{\min} as functions of the number of atomic sites in the primitive cell, N_a , are plotted in Fig.1. We associate the value of N_a with the degree of structural complexity of a compound. We see from Fig.1A that PGM- κ_L^{\min} covers a large range of values, spanning from approximately 0.01 to 1 W/[m·K] in the high temperature limit (600 K and above). There is a clear trend that PGM- κ_L^{\min} decreases monotonically with increasing N_a , which can be clearly seen from the log-log plot in the inset of Fig.1A). In contrast, the total PGM+OD- κ_L^{\min} in Fig.1B exhibits a much narrower spread from approximately 0.1 to 2.6 W/[m·K], independent of N_a . The lower (0.1 W/[m·K]) and the upper (2.6 W/[m·K]) bounds were determined by analyzing the frequency distribution histogram of all calculated κ_L^{\min} , as detailed in the Supplementary Materials section. There are only four compounds within our calculations having values of PGM+OD- κ_L^{\min} outside these bounds. The largest

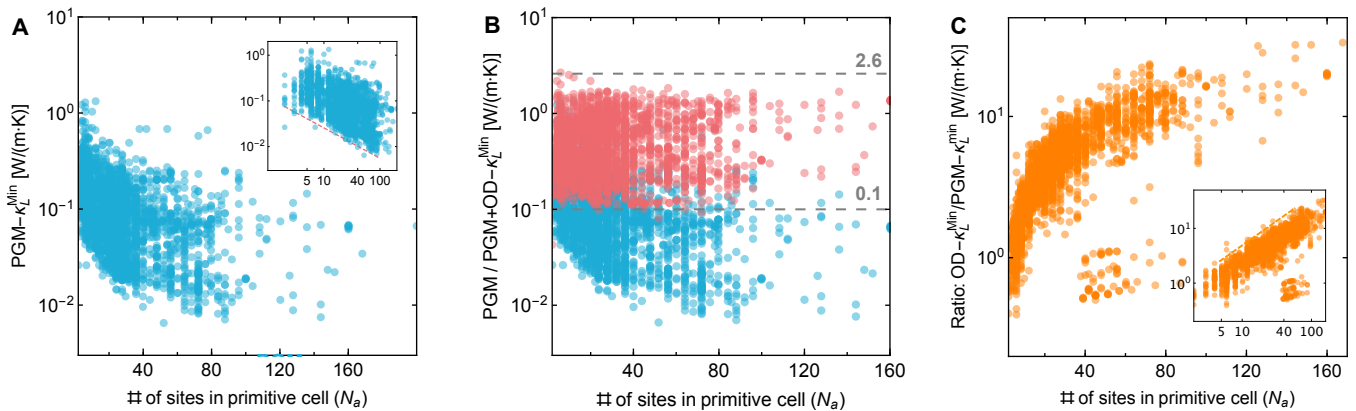


FIG. 1. Contributions to minimum lattice thermal conductivity from the phonon gas model and the off-diagonal terms based on Eq.[1]. (A) Calculated minimum lattice thermal conductivity (κ_L^{min}) as a function of the number of atomic sites (N_a) in a primitive cell using the phonon gas model (denoted as $\text{PGM-}\kappa_L^{\text{min}}$), i.e., the diagonal part of Eq.(1). The inset is plotted with logarithmic scales and the dashed line is plotted following the scaling of $N_a^{-2/3}$ obtained from Slack’s model [27], showing the monotonic decay of $\text{PGM-}\kappa_L^{\text{min}}$ with increasing N_a . (B) The same as (A) but with additional red disks showing the calculated κ_L^{min} accounting for both the PGM and off-diagonal (OD) contributions, denoted as $\text{PGM+OD-}\kappa_L^{\text{min}}$. The gray dashed lines indicate values of 0.1 and 2.6 W/[m·K] for the lower and the upper bounds of $\text{PGM+OD-}\kappa_L^{\text{min}}$, respectively. (C) The ratio of $\text{OD-}\kappa_L^{\text{min}}$ and $\text{PGM-}\kappa_L^{\text{min}}$ as a function of N_a . The inset is displayed with logarithmic scales, showing the increasing trend of $\text{OD-}\kappa_L^{\text{min}}/\text{PGM-}\kappa_L^{\text{min}}$. All results were obtained at 600 K.

deviation from the lower bound is found in crystalline $P6(3)/mmc$ -Ar, which has a value of 0.043 W/[m·K], and all the other compounds have values larger than 0.081 W/[m·K]. Meanwhile, for the upper bound, the largest $\text{PGM+OD-}\kappa_L^{\text{min}}$ is associated with $P4(2)/mnm$ -TiO₂, with a value of 2.64 W/[m·K]. The comparison of $\text{PGM-}\kappa_L^{\text{min}}$ and $\text{PGM+OD-}\kappa_L^{\text{min}}$ reveals the increasing importance of the off-diagonal diffuson term $\text{OD-}\kappa_L^{\text{min}}$ with increasing structural complexity N_a . This is further illustrated by the ratio of $\text{OD-}\kappa_L^{\text{min}}$ to $\text{PGM-}\kappa_L^{\text{min}}$ in Fig.1C. We see that $\text{OD-}\kappa_L^{\text{min}}$ quickly surpasses $\text{PGM-}\kappa_L^{\text{min}}$ above $N_a \sim 10$ and $\text{OD-}\kappa_L^{\text{min}}$ becomes an order of magnitude higher than $\text{PGM-}\kappa_L^{\text{min}}$ above $N_a \sim 60$. We also observe a group of compounds (e.g., $P3m1$ -ZnS) with ratios of $\text{OD-}\kappa_L^{\text{min}}$ to $\text{PGM-}\kappa_L^{\text{min}}$ significantly smaller than the majority trendline. Our analysis of their structures reveals that these compounds display extreme crystalline anisotropy, i.e., the lattice constant of the primitive cell along one axis is exceedingly large and thus N_a is large. However, for these compounds, the ratios of $\text{OD-}\kappa_L^{\text{min}}$ to $\text{PGM-}\kappa_L^{\text{min}}$ are reduced along the other two axes with much smaller lattice constants, thus giving rise to overall reduced ratios after averaging over the three spatial directions.

The monotonic decay of $\text{PGM-}\kappa_L^{\text{min}}$ as a function of N_a is not unexpected. As already reflected in the Slack model [27, 36], κ_L based on the PGM is proportional to $N_a^{-2/3}$ provided that acoustic phonon modes with high group velocities dominate κ_L . The monotonic decay of $\text{PGM-}\kappa_L^{\text{min}}$ can be attributed to the fact that the increase in N_a leads to a reduced Brillouin zone that effectively folds back the high-energy acoustic modes into the first Brillouin zone as optical modes, resulting in both sup-

pressed spectral weight and reduced group velocity. It is worth noting that strategies based on the above argument have been successfully used to search for complex materials with intrinsically low lattice thermal conductivity [26, 37]. However, our results show that these strategies may be no longer effective when phonons are strongly scattered by anharmonicity or disorder when the heat transport is dominated by the OD terms beyond the PGM. This is especially true for systems with κ_L approaching κ_L^{min} . In this scenario, the breakdown of the PGM is due to the crossover in the heat transport from propagating phonons to localized diffusons, as initially proposed by Allen and Feldman [15, 16]. As a result, the total $\text{PGM+OD-}\kappa_L^{\text{min}}$ provides a much more reasonable estimation of κ_L^{min} compared to the phonon term $\text{PGM-}\kappa_L^{\text{min}}$ alone. Importantly, despite such a crossover from $\text{PGM-}\kappa_L^{\text{min}}$ to $\text{OD-}\kappa_L^{\text{min}}$, the bounds of the total $\text{PGM+OD-}\kappa_L^{\text{min}}$ remain independent of N_a . This suggests an effective interconversion between the two fundamentally different heat transfer channels, which might be induced by variations in chemical composition, atomic disorder, lattice distortion, structural complexity (N_a), and other factors. This invites the following two questions: (i) what are the key factors that determine the interconversion between $\text{PGM-}\kappa_L^{\text{min}}$ and $\text{OD-}\kappa_L^{\text{min}}$ across various compounds? and (ii) is it possible to revert such a interconversion, for example, via approximating $\text{PGM+OD-}\kappa_L^{\text{min}}$ of compounds with large N_a using only $\text{PGM-}\kappa_L^{\text{min}}$?

Answering the above two questions will help establish a unified understanding of κ_L^{min} . The challenge arises from the fact that the crossover in the heat transport from phonons to diffusons is observed in a large set of

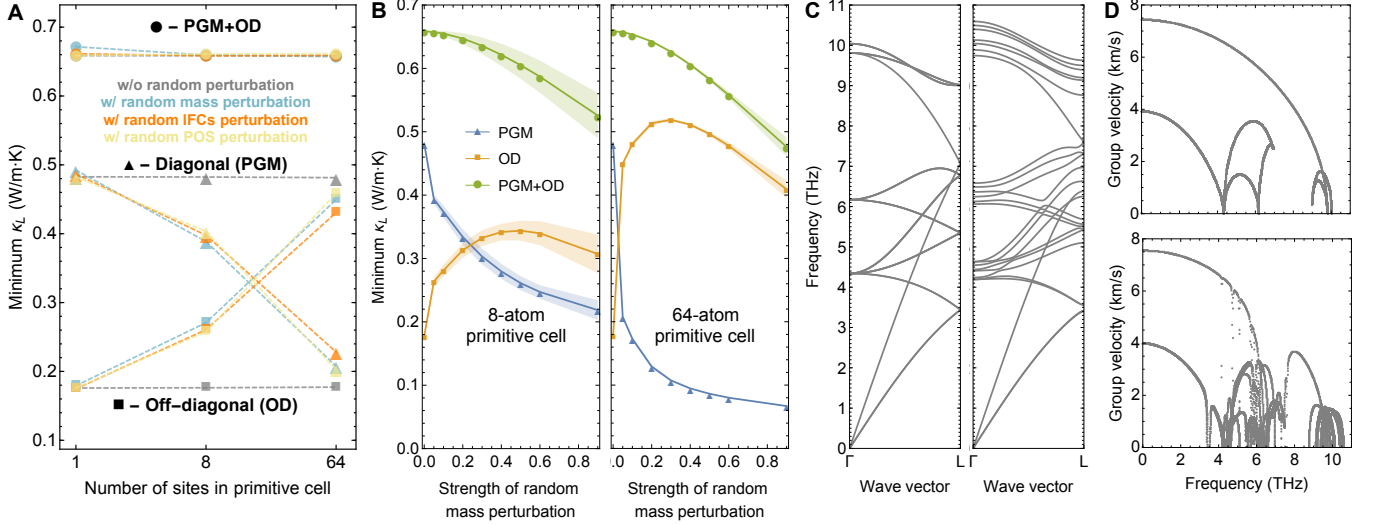


FIG. 2. Impacts of disorder and structural complexity on minimum lattice thermal conductivity. (A) Calculated total κ_L^{\min} (PGM+OD- κ_L^{\min}) and the corresponding decomposed contributions (PGM- κ_L^{\min} and OD- κ_L^{\min}) of a model system (fcc-Al) as functions of the number of atomic sites (N_a) in the designed primitive cell and the presence of various kinds of disorder. We artificially create three kinds of disorder in the perfect crystal of fcc-Al by applying small random perturbations (within 5% of their original values) to atomic mass, interatomic force constants (IFCs), and atomic position (POS), denoted in blue, orange, and yellow, respectively (with dashed line as a guide to the eye). (B) Calculated PGM+OD- κ_L^{\min} (green disks), PGM- κ_L^{\min} (blue triangles), and OD- κ_L^{\min} (orange squares) of fcc-Al as a function of the strength of mass disorder, realized by applying random percentage-wise mass perturbation. For example, 20% random mass perturbation means a random mass ranging from -20% and 20% of the original atomic mass of the element is added to each atom. The left and right panel show the results obtained for an 8-atom and 64-atom primitive cell, respectively. The shaded areas indicate the uncertainty obtained by averaging many independent random mass perturbations. (C) Phonon dispersions of the perfect fcc-Al (left panel) and an 8-atom primitive cell with 20% random mass perturbations (right panel). (D) Phonon group velocities of the perfect fcc-Al (upper panel) and an 8-atom primitive cell with 20% random mass perturbations (lower panel). The κ_L^{\min} shown in panel A and B were all calculated at 300 K.

compounds with diverse characteristics. To reveal and disentangle the impacts of chemical composition, interatomic interaction, and structural complexity on κ_L^{\min} , we use a simple elemental structure, i.e., face-centered cubic aluminium (fcc-Al), as a base model and then manually generate perturbations on this model to mimic the variations in structures and chemistries among different compounds. Specifically, random perturbations are applied on the atomic mass, interatomic force constants (IFCs), and atomic position. We also vary the number of atoms (N_a) in the unit cell by repeating the primitive cell of fcc-Al. As a consequence, we can use these models to approximate a variety of situations ranging from ordered to disordered by varying the strength of perturbations and N_a . Note that we strictly enforce physical constraints when applying these perturbations, such as the translational invariance of the crystal.

Fig. 2A summarizes the calculated total κ_L^{\min} and its decompositions (PGM and OD) when weak perturbations are applied respectively to atomic masses, IFCs, and atomic positions in unit cells with increasing N_a . First, we observe that neither the total κ_L^{\min} nor its decomposition change by simply increasing N_a without introducing disorder. This is as expected because nothing has been changed physically and merely a larger unit

cell is used as the primitive cell for the perfect fcc-Al crystal. In contrast, when small perturbations are applied, we notice different trends in PGM- κ_L^{\min} and OD- κ_L^{\min} across the unit cells with increased N_a : (i) when $N_a=1$, perturbations lead to only small changes in both PGM- κ_L^{\min} and OD- κ_L^{\min} , and the PGM- κ_L^{\min} dominates over the OD- κ_L^{\min} , as expected for a simple crystal; (ii) when $N_a=8$, perturbations start to convert PGM- κ_L^{\min} to OD- κ_L^{\min} , with the former still larger than the latter; (iii) when $N_a=64$, the values of PGM- κ_L^{\min} and OD- κ_L^{\min} are nearly exchanged, and OD- κ_L^{\min} becomes the major contribution to the total κ_L^{\min} . Surprisingly, the total κ_L^{\min} largely remains constant with both varying perturbations and N_a .

The above results reveal that the total κ_L^{\min} is not sensitive to small perturbations of atomic masses, positions, and IFCs of a given base crystal structure. In the other words, the capability of lattice heat transfer of a given system that approaches maximum phonon scattering ($\tau_{\mathbf{q}}^s \approx \pi/\omega_{\mathbf{q}}^s$) can neither be reduced nor enhanced significantly with small adjustments in atomic compositions, crystal structure, and interatomic interactions. This is in contrast to the case of weak phonon scattering in some materials (e.g. diamond and BN), wherein small mass perturbations such as isotope scattering can

lead to a considerable reduction in κ_L [38]. Conversely, the relative contributions of PGM and OD terms are very sensitive to small perturbations, especially for increasingly large unit cells. The significantly decreased PGM contribution can be mostly attributed to the reduced (diagonal) phonon group velocities. As shown in Fig.2C and D, the introduction of mass disorder strongly breaks the energy degeneracy of phonon bands and suppresses the (diagonal) group velocities, whereas phonon frequencies change by much less. This results in an increased OD contribution due to the lifting of degeneracy, which makes the otherwise vanishing off-diagonal velocities appreciable [39]. We can also infer from Fig.2A that the PGM- κ_L^{min} tends toward zero when N_a approaches infinity while OD- κ_L^{min} approaching the total κ_L^{min} . Interestingly, such a disorder-induced interconversion between PGM- κ_L^{min} and OD- κ_L^{min} , when approached from an inverse perspective, might be leveraged to estimate the total κ_L^{min} without explicitly computing the OD contributions. That is, we may approximate the total κ_L^{min} of some very complex materials (large N_a) wherein OD- κ_L^{min} dominates by computing only the PGM- κ_L^{min} of a simplified model (e.g. $N_a = 1$). The latter could be obtained by averaging the atomic masses, positions, and IFCs of the complex structure. κ_L^{min} based on such an approximation can be easily calculated using macroscopic properties such as materials' density and elastic properties.

We have so far qualitatively answered the two questions raised earlier by means of showing the impacts of weak disorder and structural complexity on κ_L^{min} in an idealized model. However, the assumption of weak disorder makes the above picture applicable to only a small group of compounds which share similar structures, chemical compositions, and interatomic interactions. To better describe complex materials with large structural and compositional fluctuations, we move on to investigate models with increasingly strong disorder. We show in Fig.2B the calculated total and decomposed κ_L^{min} as a function of the strength of random mass disorder (our tests show that perturbing IFCs has similar effects). We see from Fig.2B that PGM- κ_L^{min} decreases sharply with the onset of the disorder and then continues to decrease in a slower manner with increasing disorder. In contrast, OD- κ_L^{min} increases first and then decreases with enhanced disorder, while its percent contribution keeps increasing (see Supplementary Materials). The resulting total κ_L^{min} displays an overall reduced value. By comparing the left and right panels in Fig.2B, we also observe that a larger unit cell with similar strength of disorder tends to shift the maximum of OD- κ_L^{min} towards the weaker disorder regime and make OD- κ_L^{min} more important.

Overall, we see that, in the full range of disorder from weak to strong, the total κ_L^{min} of complex unit cells might be approximated by computing only PGM- κ_L^{min} for the perfectly ordered crystal, despite the latter displaying certain underestimation. Surprisingly, the presence of strong disorder might accidentally lead to a better agree-

ment between the two, as can be inferred by comparing OD- κ_L^{min} without any disorder and the total κ_L^{min} with strong disorder in Fig.2B. These results help explain why we find that the total PGM+OD- κ_L^{min} in Fig.1B lies in a relatively narrow range, which is bounded both from above and below over a variety of compounds. It can be interpreted as follows: (i) complex compounds are nothing but variants of simple compounds with additional compositional and structural disorder; (ii) despite potentially dissimilar amounts of structural complexity, different compounds share close values of κ_L^{min} if their averaged structural properties, such as mass, position, and interatomic interaction, are similar; (iii) it is likely that the averaged structural properties depend weakly on structural complexity for compounds with similar chemistries.

We apply these newly developed insights to bridge the knowledge gap between our κ_L^{min} model and the CWP model. This is motivated by the missing connection between the CWP model and Allen and Feldman's theory of diffusons, a question initially raised by Cahill and Pohl [12]. Considering the PGM nature of the CWP model, we first compare the PGM- κ_L^{min} calculated using our model to those from the CWP model (denoted as CWP- κ_L^{min}). To eliminate the uncertainty caused by an anisotropic average of κ_L^{min} , we only selected compounds with cubic symmetry, as shown in Fig.3A. In contrast to the expected failure of the CWP model due to the lack of OD contribution, we find that CWP- κ_L^{min} deviates significantly from PGM- κ_L^{min} and displays much larger values, which seems to overcome the underestimation inherent in PGM- κ_L^{min} . The latter is further confirmed by plotting CWP- κ_L^{min} against PGM+OD- κ_L^{min} in Fig.3B. Overall, we find that CWP- κ_L^{min} is comparable to PGM+OD- κ_L^{min} , although the latter tends to show smaller values statistically.

The above comparison reveals that the CWP model seems to work remarkably well, which is quite surprising because (i) the CWP model is relatively simple and only needs sound velocity and number density as inputs [see Eq(3) in Ref.[9]], and (ii) the CWP model does not at all account for the OD contribution, which is dominated by optical phonon modes [28]. We attribute the success of the CWP model to the fact that the CWP model could be a good approximation to the sophisticated PGM+OD- κ_L^{min} model based on Eq.(1) by averaging out disorder and phonon unfolding, in the same spirit of our model detailed earlier. This is achieved by neglecting the details of both chemical composition and atomic arrangement using a single parameter, i.e., the number density n , to describe the structure in the CWP model. In such a simplified picture with only one atom in an averaged unit cell, only three acoustic branches arise, which induces an effective back conversion from the OD contribution to the PGM contribution, thus making the PGM dominant again. This picture is supported by Fig.1C, which shows that PGM- κ_L^{min} tends to dominate over OD- κ_L^{min} in simple crystals. Importantly, the above analysis implies that it is inappropriate to use the CWP model as a

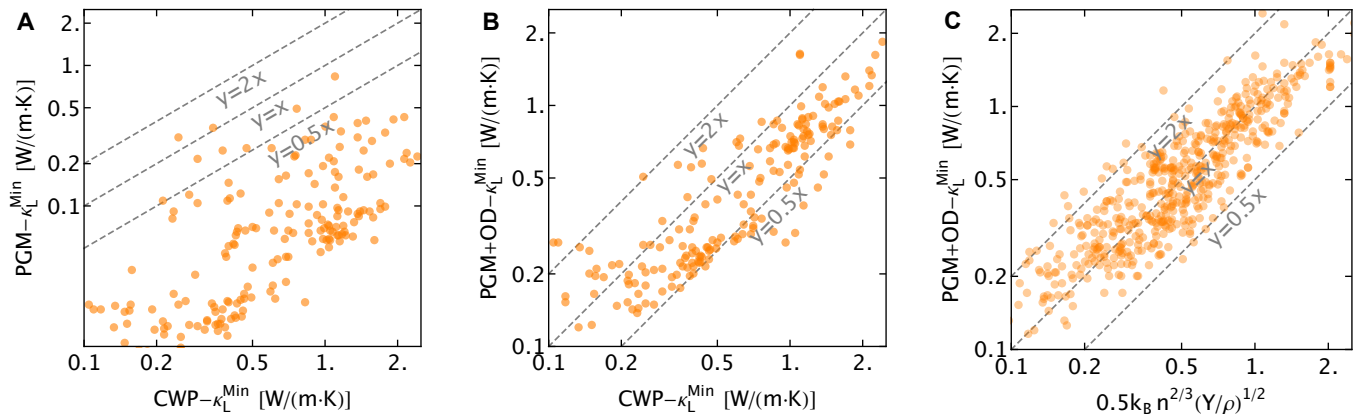


FIG. 3. Comparisons of the minimum lattice thermal conductivity based on Eq.[1] with the CWP model for cubic crystals at 600 K. (A) Comparisons of the phonon gas model of κ_L^{min} (PGM- κ_L^{min}) with the CWP model (CWP- κ_L^{min}). (B) Comparisons of the unified minimum thermal transport model that combines both phonon gas model and the off-diagonal terms (PGM+OD- κ_L^{min}) with the CWP model. (C) The linear correlation of the PGM+OD- κ_L^{min} with an approximated formula of the CWP model in the high temperature limit, i.e., $0.5k_B n^{2/3}(Y/\rho)^{1/2}$, wherein n , Y , and ρ are the number density, Young's modulus, and mass density, respectively. The dashed lines in (A), (B), and (C) denote the deviations from the diagonal within a factor of two.

second heat transport channel on top of the PGM model as adopted in recent studies [18, 40], which will result in a double-counting of the PGM contribution.

The interpretation of the CWP model based on the structure averaging and phonon unfolding picture offers additional insights into its potential limitations or uncertainties. On one hand, neglecting structural details might lead to a lack of additional flattening of phonon dispersions caused by disorder or symmetry breaking, thus giving rise to an overestimated κ_L^{min} . On the other hand, OD contributions from the three acoustic branches are still missing, which leads to a general underestimation of κ_L^{min} . Considering these two competing factors, there is no clear answer on the net effect. However, through our numerical experiment presented in Fig.3B, we see that CWP- κ_L^{min} is likely to overestimate κ_L^{min} , thus indicating that the dominant uncertainty probably comes from the first factor. This might explain why experiments tend to find lower lattice thermal conductivities than the values predicted by the CWP model [10].

To establish a quantitative measure of the extent that the CWP model overestimates κ_L^{min} compared to our model, in Fig.3C, we numerically fit our calculated PGM+OD- κ_L^{min} based on the relation of $\kappa_L^{\text{min}} \propto k_B n^{2/3}(Y/\rho)^{1/2}$ suggested by Clarke [7], wherein n is the number density, Y is Young's modulus, and ρ is the mass density. We find that PGM+OD- $\kappa_L^{\text{min}} \approx 0.5k_B n^{2/3}(Y/\rho)^{1/2}$, which is considerably smaller than that from the CWP model in the high temperature limit [9], i.e., $\kappa_L^{\text{min}} \approx 1.1k_B n^{2/3}(Y/\rho)^{1/2}$ if sound velocity is approximated as $v_s = (2v_T + v_L)/3 \approx 0.94(Y/\rho)^{1/2}$ [7, 10]. Our analysis unambiguously demonstrates that the CWP model tends to overestimate κ_L^{min} intrinsically, thus offering a different perspective from the proposal by Agne

et al. [10], who propose to mitigate such an overestimation by resorting to an alternative heat transfer through diffusons. We note that our conclusion only applies to the general behavior of the CWP model but may not work for a specific compound, as indicated by the large spread of data points along the diagonal in Fig.3C. Furthermore, we see from the relation of $\kappa_L^{\text{min}} \propto k_B n^{2/3}(Y/\rho)^{1/2}$ that the bound to κ_L^{min} of crystals can be attributed to the competing parameters of n , Y , and ρ , all of which might have physical bounds for crystals.

With our κ_L^{min} model established, we wanted to investigate the distribution of κ_L^{min} across all experimentally known compounds in the Inorganic Crystal Structure Database (ICSD) [45]. Due to the high computational cost of calculating phonon properties from first-principles, it would be unfeasible to calculate them all, making it necessary to use a more efficient model. We decided on two complementary approaches to machine-learn κ_L^{min} : MatErials Graph Network (MEGNet) [46] – a state of the art crystal graph convolutional neural network – and a random forest – a more interpretable approach (as seen in Fig.4A). MEGNet directly uses crystal structure information to construct crystal graphs as features. In contrast, the random forest requires featurization. For the random forest, we used a variety of features generated by Matminer [47] using the Magpie [48] preset including the mean, standard deviation, minimum, maximum, mode, and range of elemental properties such as atomic number (N), mass (m), electronegativity (EN), Mendeleev number (N_m), melting temperature (T_m), column, row, covalent radius (R_{covalent}), number of electrons and unfilled slots in the s , p , d , and f valence orbitals, bandgap (E_{gGS}), magnetic moment (M_{GS}), and volume per atom in the ground state (V_{GS}). We also in-

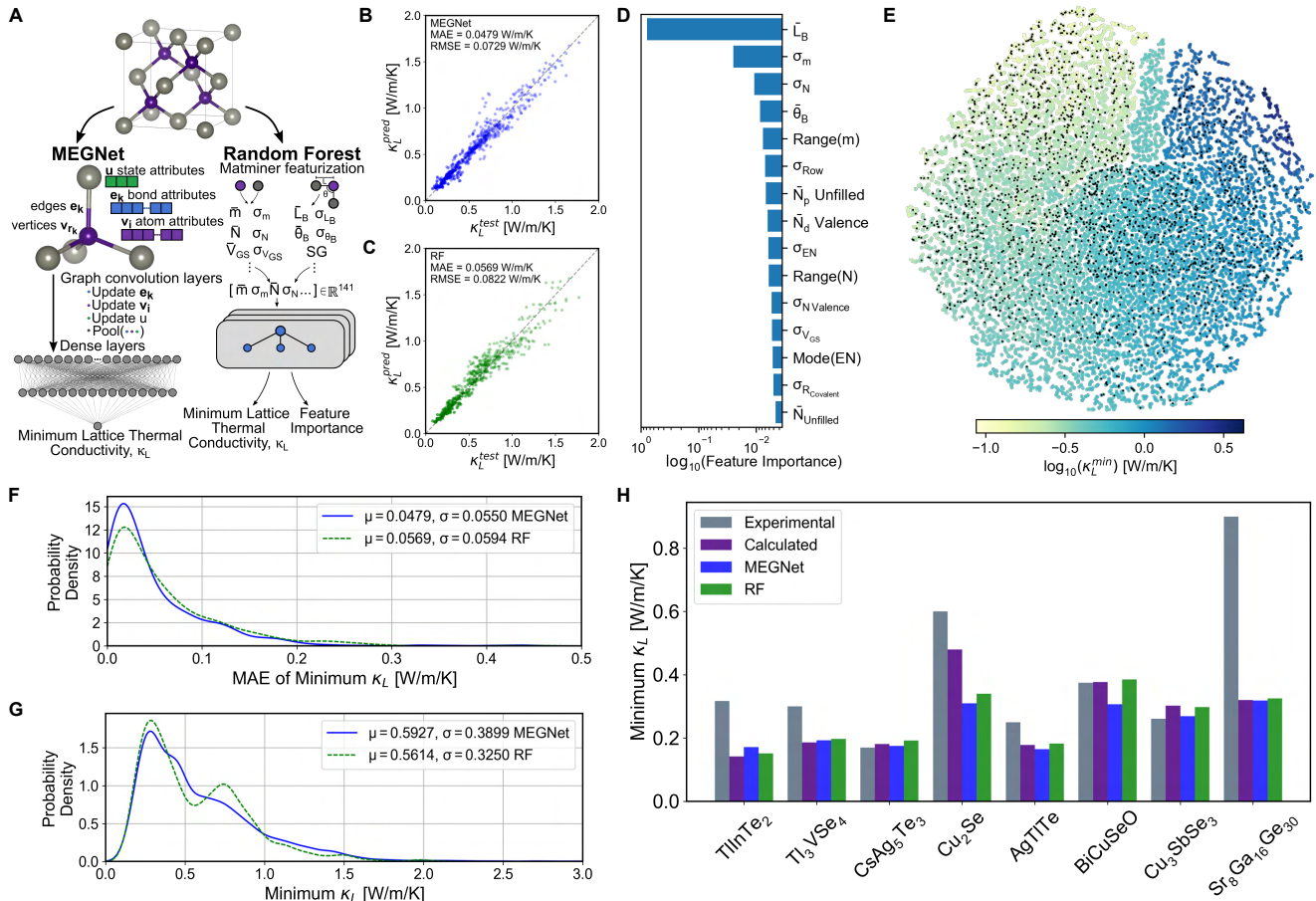


FIG. 4. Machine learning models of minimum lattice thermal conductivity. (A) Depiction of the two machine-learning models, and the error on the test set for (B) MEGNet and (C) the random forest. (D) Feature importance from the random forest. (E) MEGNet latent graph features reduced to two dimension through t-SNE. Black points show the training set and other points show the ICSD dataset, colored by their estimated κ_L^{\min} . (F) Kernel density estimate of the MAE distribution for κ_L^{\min} for both models on the test set. (G) Kernel density estimate of the κ_L^{\min} for both models on the ICSD dataset. (H) κ_L^{\min} of seven selected compounds from experiments ($TlInTe_2$ at 600 K [41], Tl_3VSe_4 at 300 K [18], $CsAg_5Te_3$ at 600 K [25], Cu_2Se at 600 K [23], $AgTlTe$ at 600 K [22], $BiCuSeO$ at 600 K [42], Cu_3SbSe_3 at 600 K [43], and $Sr_8Ga_{16}Ge_{30}$ at 300 K [44]), direct calculation using our PGM+OD- κ_L^{\min} model, MEGNet, and the random forest at the corresponding temperatures. All κ_L^{\min} were isotropically averaged.

cluded some simple structural features such as the space group, and the mean and standard deviations of both bond length (L_B) and angle (θ_B), totaling 141 features for each compound. We refer the readers to the Methods section for more details on training machine learning models.

The two models achieve similar accuracies on our test set, with MEGNet slightly outperforming the random forest (Fig. 4B,C, and F), and both also predict similar distributions for κ_L^{\min} on the ICSD data set (Fig. 4G). The distribution is bounded on the low end near 0.1 W/[m·K] and a maximum around 4 W/[m·K]. Only ~ 100 of the $\sim 36,000$ structures show MEGNet-predicted κ_L^{\min} values above 2.64 W/[m·K] (the maximum observed in the calculated training set) and are almost entirely various allotropes of Be, C, and Co or carbides and nitrides, all

having strong bonding and relatively low densities. Part of the difference in predicted values between the models arises from a limitation of the random forest, as it is restricted to interpolating between closest data points in our training set, preventing it from predicting smaller or larger values than those it was trained on. On the other hand, MEGNet is capable of extrapolation and finds more compounds with higher values of κ_L^{\min} when compared to the random forest and finds a smoother distribution for intermediate values, as shown in Fig. 4G.

The random forest model provides advantages in the form of faster computation, interpretable feature importance, and easily visualized features. From the random forest, we extracted the 15 most important features and have plotted them in Fig. 4D. Our most information-dense features are related to bonding strength (L_B , θ_B ,

EN , N_{valence}) and factors concerning the atomic properties (m , N , ρ , R_{covalent} , V_{GS}). In some cases, the mean properties are more useful, such as for bond length (L_B), bond angle (θ_B), and valence electron counts (N_{valence}), while in other cases, the differences between atomic properties carry more information (σ_m , σ_N , σ_{Row} , σ_{EN}). This is not unexpected, as phonon transport is sensitive to both similarities and differences within compounds. For example, we tend to expect shorter bonds to be stronger which results in higher characteristic frequencies, while mass difference among atoms could significantly alter the phonon spectrum. Notably, the most information-dense features being related to bonding strength is consistent with the positive correlation with Y in the relation of $\kappa_L^{\text{min}} \propto k_B n^{2/3} (Y/\rho)^{1/2}$.

Finally, we performed dimensionality reduction using t-SNE (t-Distributed Stochastic Neighbor Embedding) with PCA (Principal Component Analysis) initialization in order to project MEGNet’s latent graph features into two dimensions for visualization, as seen in Fig. 4E. The distribution of the training set and the ICSD dataset are considered together, and the overlap generally tells us how well the training set covers the ICSD dataset, indicating potential transferability of the model. The points containing ICSD materials with low and high predicted κ_L^{min} are segregated in the latent space, allowing the model to clearly separate them from each other. Additionally, the training set points span the extent of the axes and their distribution varies smoothly, with the exception of less density near some outer edges and a small cluster towards the top center of the figure. Nevertheless, the coverage is especially dense in the area of low predicted κ_L^{min} which is most relevant for thermoelectric or thermal barrier coating materials, suggesting that our training set sufficiently covers the space, but coverage could be improved by increasing the size of our training set in the future.

We further validate these predictions against experimental measurements and direct calculations using Eq. [1]. Since κ_L^{min} is relatively rare in ordered crystals, we deliberately choose thermoelectric materials exhibiting ultralow κ_L , which presumably best represent κ_L^{min} , as shown in Fig. 4H. We find that the experimental values are either higher or comparable to PGM+OD- κ_L^{min} , consistent with the definition of κ_L^{min} . It is noteworthy that compounds including CsAg_5Te_3 [25], Cu_3SbSe_3 [43], and BiCuSeO [42] have κ_L already close to κ_L^{min} from our model, suggesting that further improvement in thermoelectric efficiency should be focused on optimizing their electronic transport properties. We note that CsAg_5Te_3 and Cu_3SbSe_3 indeed resemble amorphous solids and display nearly temperature-independent and glasslike κ_L [25, 43]. Whereas for compounds such as Tl_3VSe_4 [18] and TlInTe_2 [41], there is still room for further reducing κ_L , although their κ_L are already very low. Also, we find it interesting to see a large gap between our calculated κ_L^{min} and the experimentally measured κ_L in $\text{Sr}_8\text{Ga}_{16}\text{Ge}_{30}$ [44, 49], a typical electron-crystal phonon-

glass material. This finding implies that although κ_L of a material might exhibit a temperature dependence similar to that of glasses, κ_L may still not achieve the minimum.

Overall, the machine-learned κ_L^{min} from both MEGNet and the random forest agree very well with our direct calculations. This is rather encouraging because most of the compounds are not contained in the training dataset for the machine learning models except for TlInTe_2 . The largest deviation between experiment, machine learning models, and direct calculation is found in Cu_2Se . The discrepancy might be attributed to the following factors: (i) we used an ordered structure ($\beta\text{-Cu}_2\text{Se}$) to compute κ_L^{min} , while in the experimental structure the copper ions are highly disordered around the Se sublattice [23]; (ii) $\beta\text{-Cu}_2\text{Se}$ often exhibits off-stoichiometry with copper vacancies, resulting in relatively large variations in the experimentally measured values of κ_L in the range of 0.4-0.6 W/[m·K] among different samples [23]. Therefore, despite the disordered nature of $\beta\text{-Cu}_2\text{Se}$, our models, including both machine learning and direct calculation, seem to provide reasonable estimations using ordered structures.

The above results on Cu_2Se indicate that κ_L of amorphous compounds might be approximated with a reasonable accuracy using ordered crystals. To confirm this hypothesis, we further apply our model to amorphous silica ($\alpha\text{-SiO}_2$). We calculated PGM+OD- κ_L^{min} for two ordered phases of SiO_2 ($\alpha\text{-quartz}$ and $\alpha\text{-cristobalite}$) that are free of lattice instabilities, which are compared to the CWP model and the experimental measurement [9] in Fig. 5A. We see that PGM+OD- κ_L^{min} of both $\alpha\text{-quartz}$ and $\alpha\text{-cristobalite}$ agree well with experiment, displaying overall improvement over the CWP model, particularly at high temperatures. This implies that specific atomic arrangement might not be very relevant when approaching κ_L^{min} , although it is responsible for subtle differences, which are probably more profound at low temperatures.

To provide more evidence for this observation, we next examine other phases of SiO_2 using our machine learning model. Particularly, we used MEGNet instead of the random forest because the former better encodes structural information. Since our MEGNet model is trained on structures from the Materials Project (MP) [33–35], we collected all structures with the chemical formula SiO_2 available within MP, totaling 317 structures. The calculated κ_L^{min} using MEGNet is shown in Fig. 5B. We find a relatively large spread of κ_L^{min} when N_a is small ($N_a < 25$), while the spread becomes much smaller when N_a is large ($N_a > 75$). The mean value of κ_L^{min} of the 317 structures is 1.45 W/[m·K], close to the experimental value of 1.65 W/[m·K] for the amorphous phase [9] and better than the value of 1.18 W/[m·K] from the CWP model at 600 K [9]. These results confirm our earlier hypothesis that κ_L of amorphous compounds can be approximated by ordered crystals. Moreover, a reliable prediction may be achieved by averaging over different structures, effectively capturing the distinct local structures in

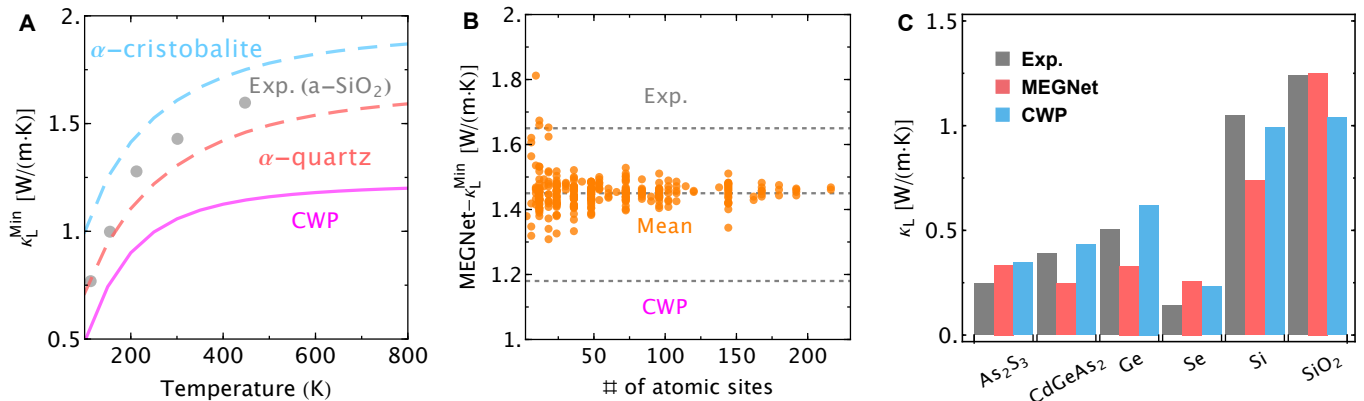


FIG. 5. Prediction of lattice thermal conductivity in amorphous solids using machine learning models of minimum lattice thermal conductivity. (A) Comparison of temperature-dependent κ_L of amorphous silica ($a\text{-SiO}_2$) between the experiment (gray disks) [9] and theoretical κ_L^{min} (solid/dashed lines). Results from the CWP model are indicated by solid magenta lines. The dashed lines display the calculated PGM+OD- κ_L^{min} for two ordered phases of SiO_2 , namely α -quartz and α -cristobalite. (B) Predicted κ_L^{min} (orange disks) at 600 K using MEGNet for 317 structures of ordered SiO_2 from Materials Project [33] as a function of the number of atomic sites in a primitive cell. The upper, middle, and lower dashed lines denote the values from the experiment, mean of MEGNet predictions, and the CWP model, respectively. (C) Comparison of κ_L at 300 K of six amorphous compounds between experiments [9], our MEGNet model, and the CWP model [9].

amorphous solids.

We apply our MEGNet model to other amorphous solids by averaging over ordered phases and compared to the experiments and the CWP model in Fig.5C. Our machine learning model achieves an accuracy comparable with the CWP model. The advantage of our model is the calculation requires very low computational cost (within a second for each compound) and simple input (only structural information), and thus is readily applicable to many other compounds on a large scale. We note that compared to the amorphous SiO_2 our predicted κ_L of amorphous Si is considerably smaller than both the CWP model and the experiment. We attribute such a discrepancy mainly to the observations reported in the literature that (i) propagating modes contribute significantly more in amorphous Si than amorphous SiO_2 , and (ii) phonon lifetimes in amorphous Si are notably larger than π/ω [50], both of which indicate that κ_L in amorphous Si still does not reach the minimum value. We hypothesize that this might also be the case for amorphous CdGeAs_2 and Ge.

Before closing, we briefly comment on the limitations of our theoretical and machine learning models. Firstly, both the identified lower bound to κ_L^{min} and the constructed machine learning models are based on the isotropically averaged κ_L^{min} . Consequently, it is reasonable to question how κ_L^{min} behaves in anisotropic structures. This anisotropy is of particular interest because κ_L as small as $0.05 \text{ W}/[\text{m}\cdot\text{K}]$ below our isotropically averaged lower bound at room temperature has been realized in layered WSe_2 crystals [51]. Therefore, we analyzed the anisotropic κ_L^{min} for all of the calculated compounds (see Fig.S3 in Supplementary Materials). We find there are 67 compounds in total that have κ_L^{min} less than 0.1

$\text{W}/[\text{m}\cdot\text{K}]$ in at least one of the three Cartesian directions. However, there are only 5 compounds exhibiting κ_L^{min} less than $0.07 \text{ W}/[\text{m}\cdot\text{K}]$ (see listed compounds and κ_L^{min} in Supplementary Materials). This observation suggests that, even though it may be difficult to find such materials due to their rarity, anisotropic materials, including layered crystals, have the potential to achieve a lattice thermal conductivity of less than $0.1 \text{ W}/[\text{m}\cdot\text{K}]$, consistent with the prior work [51].

Secondly, we computed all κ_L^{min} using the harmonic phonon dispersion in the absence of finite temperature induced phonon frequency shifts; the latter are important in a range of low-thermal-conductivity materials [52, 53]. As a first attempt to investigate the effects of phonon anharmonicity on κ_L^{min} , we computed κ_L^{min} at 300 K for Tl_3VSe_4 using harmonic and anharmonic phonon dispersions, respectively. The anharmonic phonon dispersion was computed using the self-consistent phonon theory at 300 K in a previous study [52]. We find that accounting for anharmonic effects only leads to a small change (about 7% decrease) in κ_L^{min} , which is much smaller than the change (about 162.5% increase) in κ_L when phonon lifetimes are limited by intrinsic three phonon scattering [52]. The relative insensitivity of κ_L^{min} to anharmonic effects can be explained by the relationship $\kappa_L^{\text{min}} \propto k_B n^{2/3} (Y/\rho)^{1/2} \propto k_B n^{2/3} v_s$ [7], which indicates that κ_L^{min} is largely unchanged unless anharmonic effects lead to a sizable change in sound velocity v_s .

Thirdly, it is not entirely justified to use one half of the vibrational period as the minimum phonon lifetime, i.e., $\tau = \pi/\omega$. The adoption of $\tau = \pi/\omega$ was first proposed by Cahill, Watson, and Pohl [9], motivated by Einstein's thermal conductivity model [13]. Specifically, Einstein's model relies on a critical assumption that there is no co-

herence between the motions of neighboring atoms, which seems to be a reasonable choice for glassy materials. Einstein further derived the energy exchange between neighboring atoms by integrating over one half of a period of oscillation, however, without an explicit explanation in his original paper [13]. We hypothesize this might be motivated by the fact that it is the shortest time period that an atom returns to its original position after exchanging energy with neighboring atoms. Cahill *et al.* interpreted Einstein's result to mean that each atom undergoes a thermal energy loss or gain in the span of half an oscillation period [9] and subsequently assumed that $\tau = \pi/\omega$. Mathematically, τ adopted in computing κ_L^{min} can have an arbitrary value, which presumably is small in order to reduce the PGM contribution. However, physically, τ cannot be arbitrarily short because our derived equation for κ_L^{min} relies on a critical assumption that phonons are well-behaved quasiparticles ($\tau\omega \approx 2\pi$). The very small τ implies strong interactions and will invalidate the quasiparticle picture, making the phonon properties (such as group velocities and frequencies) less well-defined and invalidating the usage of Eq.[1]. To explore the potential uncertainty due to the adopted τ , we performed sensitivity analysis of κ_L^{min} by varying τ for a randomly selected set of compounds (see Supplementary Materials). We find that κ_L^{min} decreases for most compounds when τ is decreased. Specifically, a sharp decrease in κ_L^{min} is found when τ is reduced from a larger value to π/ω , a value we adopted for computing κ_L^{min} . When τ is less than π/ω , slower decrease or no change in κ_L^{min} is observed, especially for lower values of κ_L^{min} . Since τ cannot be arbitrarily small as argued previously, we hypothesize that $\tau = \pi/\omega$ might be a reasonable choice to achieve a relatively low value of κ_L^{min} while approaching the limit of the quasiparticle picture.

Finally, despite encouraging results from the comparison between the calculations and the experiments, our theoretical model only accounts for harmonic heat flux [39, 54] and Eq.[1] fails to describe phonon satellite structures deviating from the quasiparticle picture [55]. For the machine learning model, local structural motifs may not be well captured by ordered structures for amorphous solids, and our simple averaging scheme with equal weight for each structure is probably not optimal. We deem establishing a more reliable physical bound to phonon lifetime, including higher-order anharmonic effects on the phonon frequency shifts and the heat flux beyond the phonon quasiparticle picture, and machine learning structural motifs inherent in amorphous solids are interesting avenues of further research to improve our model.

III. CONCLUSIONS

In summary, we have developed a first-principles minimum lattice thermal conductivity model based on a unified theory of thermal transport in crystals and glasses. By applying such a model to thousands of crystalline compounds, we have discovered a universal bound to minimum lattice thermal conductivity independent of structural complexity. In striking contrast to the conventional phonon gas model, such an unusual behavior is found to be deeply rooted in the conversion of the heat transfer mechanism from the phonon gas model to the diffuson picture with the presence of disorder, while the value of the total minimum lattice thermal conductivity largely remains unchanged. With these insights, we bridge the knowledge gap between the Cahill-Watson-Pohl model and our unified model by pointing out that the former could be viewed as an approximation of the latter. We further construct machine learning models based on a graph network and random forest to enable fast and accurate prediction of minimum lattice thermal conductivity on a large scale, which is validated against thermoelectric materials with ultralow and glasslike lattice thermal conductivity. We demonstrate the applicability of our graph network model to simulate lattice thermal conductivity in amorphous solids. These findings highlight a unified understanding of the lower limit of lattice thermal transport in solids. The first-principles-based theory and machine learning model built in this work are universal and readily applicable in research relevant to thermal energy conversion and management.

ACKNOWLEDGMENTS

Y.X., D.G., K.P., and C.W. acknowledge financial support received from (i) Toyota Research Institute (TRI) through the Accelerated Materials Design and Discovery program (thermal conductivity calculations), (ii) the Department of Energy, Office of Science, Basic Energy Sciences under grant DE-SC0014520 (theory of anharmonic phonons), and (iii) the U.S. Department of Commerce and National Institute of Standards and Technology as part of the Center for Hierarchical Materials Design (CHiMaD) under award no. 70NANB14H012 (DFT calculations). Y. X. was also supported by Portland State University Lab Setup Fund. M.G.K. were supported in part by the National Science Foundation Grant DMR-2003476. V.O. acknowledges financial support from the National Science Foundation Grant DMR-1611507. We acknowledge the computing resources provided by (i) the National Energy Research Scientific Computing Center (NERSC), a U.S. Department of Energy Office of Science User Facility operated under Contract No. DEAC02-05CH11231, (ii) Quest high-performance computing facility at Northwestern University which is jointly supported by the Office of the Provost, the Office for Research, and Northwestern Uni-

versity Information Technology, and (iii) Bridges2 at Pittsburgh Supercomputing Center (PSC) through allocations dmr160027p and mat220007p from the Advanced Cyber-infrastructure Coordination Ecosystem: Services & Support (ACCESS) program, which is supported by National Science Foundation grants #2138259, #2138286, #2138307, #2137603, and #2138296. The authors (Y.X., C.W, and M.K, initial DFT and conception of research problem) also acknowledge support for the initial stages of this research from the U.S. Department of Energy under Contract No. DE-SC0014520.

Appendix A: First-principles calculation of κ_L^{\min}

The key ingredients for modeling κ_L^{\min} based on Eq.[1] from first principles are materials harmonic vibrational spectra, which can be explicitly calculated if materials structure and harmonic interatomic force constants are known. To construct a large database for κ_L^{\min} , we used the phonon database (phononDB) generated by Togo [31], who used crystalline structures from the Materials Project (MP) [33–35] and calculated harmonic interactions using Phonopy [32]. It is worth noting that these phonon calculations were performed by means of the Vienna *Ab Initio* Simulation Package (VASP) [56–59], which employed the projector-augmented wave (PAW) [60] method in conjunction with the revised Perdew-Burke-Ernzerhof version (PBEsol [61]) of the generalized gradient approximation (GGA) [62] for the exchange-correlation functional [63]. We performed post processing of the phononDB (version of 2018-04-17) to generate harmonic force constants and downselected the compounds that are free of lattice instabilities (imaginary phonon frequencies) with supercell structures constructed from diagonal matrices (required by our κ_L^{\min} implementation within ShengBTE [64]), totaling 2576 compounds. These compounds cover wide ranges of chemical compositions and space group symmetries, with 189, 922, 310, 660, and 495 compounds from cubic, orthorhombic, tetragonal, trigonal/hexagonal, triclinic/monoclinic crystal systems, respectively. Other compounds and their harmonic phonon properties, including TlInTe_2 , Tl_3VSe_4 , CsAg_5Te_3 , Cu_2Se , TlAgTe , CuBiSeO , SnSe , α -cristobalite, and α -quartz, were calculated following the similar DFT settings. For β - Cu_2Se which has imaginary phonon frequencies, we have performed anharmonic phonon renormalization at finite temperature (600 K) using self-consistent phonon theory [52, 53, 65, 66].

We implemented the κ_L^{\min} model based on Eq.[1] within ShengBTE [64]. The off-diagonal group velocities were calculated following the derivations by Allen and Feldman [16] and Simoncelli *et al.* [28]. We calculated κ_L^{\min} for these 2576 compounds at three temperatures of 300 K, 600 K, and 900 K using a constant mesh density (mesh_density = 50) following Phonopy conventions [32]. The convergence is carefully monitored across different compounds to achieve good balance between accuracy

and efficiency.

Appendix B: Machine learning models

MEGNet: For the MEGNet model, we used frozen initial atom embeddings transferred from another MEGNet model [46] trained on 133,420 formation energies from Materials Project [33]. Crystal graphs were constructed using 50 features per bond with a gaussian smearing width of 0.5 Å up to a cutoff radius of 5 Å for the bond attributes, transferred atom embedding weights of size 16 for the atom attributes, and one single global attribute embedding the temperature in Kelvin. For the model hyperparameters, we used only a single MEGNet block and set the number of dense layers in the MEGNet block to $n_1 = 16$, $n_2 = 16$, and $n_3 = 8$, followed by 2 Set2Set passes, and the learning rate was set to 10^{-3} . In order to prevent overfitting, we set weight dropout to 25% during both training and prediction and added a small L2 weight regularization parameter of 10^{-5} . The κ_L^{\min} data was split 80%:10%:10% into a training set, validation set, and testing set. Predictions were then run over 10 trials and the average was taken as the final output. The model was run for 500 epochs with a patience of 250, and the model with the best validation performance was selected for further predictions. The MEGNet training mean absolute error (MAE) was 0.033 W/[m·K], the validation MAE was 0.0406 W/[m·K], and the testing MAE was 0.0479 W/[m·K]. Finally, we performed dimensionality reduction on the combined phononDB and ICSD dataset using t-SNE to project the latent graph features into 2 dimensions. We initialized the t-SNE with PCA and chose the settings of 1,000 iterations, a perplexity of 5, and a learning rate of 39,514 (n).

Random Forest: Features for the random forest were created through Matminer [47] using the Magpie preset [48], along with global symmetry features and site statistic fingerprints, totaling 141 features for each compound as detailed in the main text. The random forest was constructed using 1,000 estimators, and we verified that including more estimators did not improve the accuracy significantly. For this model, we used 5-fold cross validation on the 90% training set for parameter selection and left a holdout test set of 10%. In order to prevent overfitting, we changed the allowable maximum depth of each tree, where larger maximum depths showed better prediction accuracies at the cost of a larger gap between training and testing accuracies. A maximum depth 8 was then chosen to balance training, validation, and testing accuracy. For the random forest, the mean training MAE was 0.0375 W/[m·K], mean validation MAE was 0.0458 W/[m·K], and the testing MAE was 0.0570 W/[m·K]. Feature importance was extracted from a random forest trained on only 600 K data.

The training dataset used in both MEGNet and random forest models consists of our calculated κ_L^{\min} at three temperatures of 300K, 600K, and 900K, totaling

7728 datapoints. For the ICSD dataset, 36,199 crystal structures were pulled from the Open Quantum Materials Database (OQMD) [67, 68], and all machine learning predictions of κ_L^{min} were then performed at 600 K unless otherwise specified.

Appendix C: Data availability

The codes, data sets, and machine learning models are available via public repository (<https://github.com/yimavxia/Minikappa>)

-
- [1] Lon E. Bell, Cooling, Heating, Generating Power, and Recovering Waste Heat with Thermoelectric Systems, *Science* **321**, 1457–1461 (2008).
- [2] Glen A Slack, The thermal conductivity of nonmetallic crystals, *Solid state physics* **34**, 1–71 (1979).
- [3] G. A. Slack, *CRC Handbook of Thermoelectrics* (CRC Press, Boca Raton, FL, 1995) pp. 407–440.
- [4] G. Jeffrey Snyder and Eric S. Toberer, Complex thermoelectric materials, *Nat. Mater.* **7**, 105–114 (2008).
- [5] Joseph R Sootsman, Duck Young Chung, and Mercouri G Kanatzidis, New and old concepts in thermoelectric materials, *Angewandte Chemie International Edition* **48**, 8616–8639 (2009).
- [6] Jian He and Terry M. Tritt, Advances in thermoelectric materials research: Looking back and moving forward, *Science* **357** (2017), 10.1126/science.aak9997.
- [7] David R. Clarke, Materials selection guidelines for low thermal conductivity thermal barrier coatings, *Surface and Coatings Technology* **163-164**, 67–74 (2003), proceedings of the 29th International conference on Metallurgical Coatings and Thin Films.
- [8] Jayant Gopal Thakare, Chandan Pandey, MM Mahapatra, and Rahul S Mulik, Thermal barrier coatings—A state of the art review, *Metals and Materials International* **27**, 1947–1968 (2021).
- [9] David G. Cahill, S. K. Watson, and R. O. Pohl, Lower limit to the thermal conductivity of disordered crystals, *Phys. Rev. B* **46**, 6131–6140 (1992).
- [10] Matthias T. Agne, Riley Hanus, and G. Jeffrey Snyder, Minimum thermal conductivity in the context of diffuson-mediated thermal transport, *Energy Environ. Sci.* **11**, 609–616 (2018).
- [11] D G Cahill and R O Pohl, Lattice Vibrations and Heat Transport in Crystals and Glasses, *Annual Review of Physical Chemistry* **39**, 93–121 (1988).
- [12] David G. Cahill and R.O. Pohl, Heat flow and lattice vibrations in glasses, *Solid State Communications* **70**, 927–930 (1989).
- [13] A. Einstein, Elementare Betrachtungen über die thermische Molekularbewegung in festen Körpern, *Annalen der Physik* **340**, 679–694 (1911).
- [14] C. Kittel, *Introduction to Solid State Physics* (Wiley, 2004).
- [15] Philip B. Allen and Joseph L. Feldman, Thermal Conductivity of Glasses: Theory and Application to Amorphous Si, *Phys. Rev. Lett.* **62**, 645–648 (1989).
- [16] Philip B. Allen and Joseph L. Feldman, Thermal conductivity of disordered harmonic solids, *Phys. Rev. B* **48**, 12581–12588 (1993).
- [17] Philip B Allen, Joseph L Feldman, Jaroslav Fabian, and Frederick Wooten, Diffusons, locons and propagons: Character of atomic vibrations in amorphous Si, *Philosophical Magazine B* **79**, 1715–1731 (1999).
- [18] Saikat Mukhopadhyay, David S. Parker, Brian C. Sales, Alexander A. Puretzky, Michael A. McGuire, and Lucas Lindsay, Two-channel model for ultralow thermal conductivity of crystalline Ti_3VSe_4 , *Science* **360**, 1455–1458 (2018).
- [19] Yixiu Luo, Xiaolong Yang, Tianli Feng, Jingyang Wang, and Xiulin Ruan, Vibrational hierarchy leads to dual-phonon transport in low thermal conductivity crystals, *Nature Communications* **11**, 2554 (2020).
- [20] Yi Xia, Vidvuds Ozoliņš, and Chris Wolverton, Microscopic Mechanisms of Glasslike Lattice Thermal Transport in Cubic $\text{Cu}_{12}\text{Sb}_4\text{S}_{13}$ Tetrahedrites, *Phys. Rev. Lett.* **125**, 085901 (2020).
- [21] Riley Hanus, Janine George, Max Wood, Alexander Bonkowski, Yongqiang Cheng, Douglas L. Abernathy, Michael E. Manley, Geoffroy Hautier, G. Jeffrey Snyder, and Raphaël P. Hermann, Uncovering design principles for amorphous-like heat conduction using two-channel lattice dynamics, *Materials Today Physics* **18**, 100344 (2021).
- [22] Ken Kurosaki, Atsuko Kosuga, Keita Goto, Hiroaki Muta, and Shinsuke Yamanaka, Ag_9TlTe_5 and AgTlTe : high ZT materials with extremely low thermal conductivity, in *ICT 2005. 24th International Conference on Thermoelectrics, 2005*. (IEEE, 2005) pp. 323–326.
- [23] Huili Liu, Xun Shi, Fangfang Xu, Linlin Zhang, Wenqing Zhang, Lidong Chen, Qiang Li, Ctirad Uher, Tristan Day, and G. Jeffrey Snyder, Copper ion liquid-like thermoelectrics, *Nature Materials* **11**, 422–425 (2012).
- [24] Xu Lu, Donald T. Morelli, Yi Xia, Fei Zhou, Vidvuds Ozolins, Hang Chi, Xiaoyuan Zhou, and Ctirad Uher, High Performance Thermoelectricity in Earth-Abundant Compounds Based on Natural Mineral Tetrahedrites, *Advanced Energy Materials* **3**, 342–348 (2013).
- [25] Hua Lin, Gangjian Tan, Jin-Ni Shen, Shiqiang Hao, Li-Ming Wu, Nicholas Calta, Christos Malliakas, Si Wang, Ctirad Uher, Christopher Wolverton, and Mercouri G. Kanatzidis, Concerted Rattling in CsAg_5Te_3 Leading to Ultralow Thermal Conductivity and High Thermoelectric Performance, *Angewandte Chemie International Edition* **55**, 11431–11436 (2016).
- [26] Siqi Lin, Wen Li, Shasha Li, Xinyue Zhang, Zhiwei Chen, Yidong Xu, Yue Chen, and Yanzhong Pei, High Thermoelectric Performance of Ag_9GaSe_6 Enabled by Low Cutoff Frequency of Acoustic Phonons, *Joule* **1**, 816–830 (2017).
- [27] Glen A Slack, Nonmetallic crystals with high thermal conductivity, *Journal of Physics and Chemistry of Solids* **34**, 321–335 (1973).
- [28] Michele Simoncelli, Nicola Marzari, and Francesco Mauri, Unified theory of thermal transport in crystals and glasses, *Nature Physics* **15**, 809–813 (2019).
- [29] Leyla Isaeva, Giuseppe Barbalinardo, Davide Donadio, and Stefano Baroni, Modeling heat transport in crystals

- and glasses from a unified lattice-dynamical approach, *Nature Communications* **10**, 3853 (2019).
- [30] Michele Simoncelli, Nicola Marzari, and Francesco Mauri, Wigner Formulation of Thermal Transport in Solids, *Phys. Rev. X* **12**, 041011 (2022).
- [31] Atsushi Togo, Phonon database at Kyoto university, <http://phonondb.mtl.kyoto-u.ac.jp/> (2018).
- [32] Atsushi Togo and Isao Tanaka, First principles phonon calculations in materials science, *Scripta Materialia* **108**, 1 – 5 (2015).
- [33] Anubhav Jain, Shyue Ping Ong, Geoffroy Hautier, Wei Chen, William Davidson Richards, Stephen Dacek, Shreyas Cholia, Dan Gunter, David Skinner, Gerbrand Ceder, and Kristin A. Persson, Commentary: The Materials Project: A materials genome approach to accelerating materials innovation, *APL Materials* **1**, 011002 (2013), <https://doi.org/10.1063/1.4812323>.
- [34] Shyue Ping Ong, William Davidson Richards, Anubhav Jain, Geoffroy Hautier, Michael Kocher, Shreyas Cholia, Dan Gunter, Vincent L. Chevrier, Kristin A. Persson, and Gerbrand Ceder, Python Materials Genomics (pymatgen): A robust, open-source python library for materials analysis, *Computational Materials Science* **68**, 314–319 (2013).
- [35] Shyue Ping Ong, Shreyas Cholia, Anubhav Jain, Miriam Brafman, Dan Gunter, Gerbrand Ceder, and Kristin A. Persson, The Materials Application Programming Interface (API): A simple, flexible and efficient API for materials data based on REpresentational State Transfer (REST) principles, *Computational Materials Science* **97**, 209–215 (2015).
- [36] Glen A Slack, The thermal conductivity of nonmetallic crystals, *Solid state physics* **34**, 1–71 (1979).
- [37] Eric S. Toberer, Alex Zevalkink, and G. Jeffrey Snyder, Phonon engineering through crystal chemistry, *J. Mater. Chem.* **21**, 15843–15852 (2011).
- [38] Ke Chen, Bai Song, Navaneetha K. Ravichandran, Qiye Zheng, Xi Chen, Hwijong Lee, Haoran Sun, Sheng Li, Geethal Amila Gamage Udalamatta Gamage, Fei Tian, Zhiwei Ding, Qichen Song, Akash Rai, Hanlin Wu, Pawan Koirala, Aaron J. Schmidt, Kenji Watanabe, Bing Lv, Zhifeng Ren, Li Shi, David G. Cahill, Takashi Taniguchi, David Broido, and Gang Chen, Ultrahigh thermal conductivity in isotope-enriched cubic boron nitride, *Science* **367**, 555–559 (2020), <https://www.science.org/doi/pdf/10.1126/science.aaz6149>.
- [39] Robert J. Hardy, Energy-Flux Operator for a Lattice, *Phys. Rev.* **132**, 168–177 (1963).
- [40] Minghui Wu, Enamullah, and Li Huang, Unusual lattice thermal conductivity in the simple crystalline compounds TiXTe_2 ($\text{X}=\text{Ga}, \text{In}$), *Phys. Rev. B* **100**, 075207 (2019).
- [41] Manoj K. Jana, Koushik Pal, Avinash Warankar, Pankaj Mandal, Umesh V. Waghmare, and Kanishka Biswas, Intrinsic Rattler-Induced Low Thermal Conductivity in Zintl Type TlInTe_2 , *Journal of the American Chemical Society*, *Journal of the American Chemical Society* **139**, 4350–4353 (2017).
- [42] Yan-Ling Pei, Haijun Wu, Di Wu, Fengshan Zheng, and Jiaqing He, High Thermoelectric Performance Realized in a BiCuSeO System by Improving Carrier Mobility through 3D Modulation Doping, *Journal of the American Chemical Society*, *Journal of the American Chemical Society* **136**, 13902–13908 (2014).
- [43] Kriti Tyagi, Bhasker Gahtori, Sivaiah Bathula, A. K. Srivastava, A. K. Shukla, Sushil Auluck, and Ajay Dhar, Thermoelectric properties of Cu_3SbSe_3 with intrinsically ultralow lattice thermal conductivity, *J. Mater. Chem. A* **2**, 15829–15835 (2014).
- [44] G. S. Nolas, J. L. Cohn, G. A. Slack, and S. B. Schujman, Semiconducting Ge clathrates: Promising candidates for thermoelectric applications, *Applied Physics Letters* **73**, 178–180 (1998), <https://doi.org/10.1063/1.121747>.
- [45] Alec Belsky, Mariette Hellenbrandt, Vicky Lynn Karen, and Peter Luksch, New developments in the Inorganic Crystal Structure Database (ICSD): accessibility in support of materials research and design, *Acta Crystallographica Section B: Structural Science* **58**, 364–369 (2002).
- [46] Chi Chen, Weike Ye, Yunxing Zuo, Chen Zheng, and Shyue Ping Ong, Graph Networks as a Universal Machine Learning Framework for Molecules and Crystals, *Chemistry of Materials* **31**, 3564–3572 (2019), <https://doi.org/10.1021/acs.chemmater.9b01294>.
- [47] Logan Ward, Alexander Dunn, Alireza Faghaninia, Nils E.R. Zimmermann, Saurabh Bajaj, Qi Wang, Joseph Montoya, Jiming Chen, Kyle Bystrom, Maxwell Dylla, Kyle Chard, Mark Asta, Kristin A. Persson, G. Jeffrey Snyder, Ian Foster, and Anubhav Jain, Matminer: An open source toolkit for materials data mining, *Computational Materials Science* **152**, 60–69 (2018).
- [48] Logan Ward, Ankit Agrawal, Alok Choudhary, and Christopher Wolverton, A general-purpose machine learning framework for predicting properties of inorganic materials, *npj Computational Materials* **2**, 16028 (2016).
- [49] B.C. Chakoumakos, B.C. Sales, D.G. Mandrus, and G.S. Nolas, Structural disorder and thermal conductivity of the semiconducting clathrate $\text{Sr}_8\text{Ga}_{16}\text{Ge}_{30}$, *Journal of Alloys and Compounds* **296**, 80–86 (2000).
- [50] Jason M. Larkin and Alan J. H. McGaughey, Thermal conductivity accumulation in amorphous silica and amorphous silicon, *Phys. Rev. B* **89**, 144303 (2014).
- [51] Catalin Chiritescu, David G Cahill, Ngoc Nguyen, David Johnson, Arun Bodapati, Pawel Koblinski, and Paul Zschack, Ultralow thermal conductivity in disordered, layered WSe_2 crystals, *Science* **315**, 351–353 (2007).
- [52] Yi Xia, Koushik Pal, Jiangang He, Vidvuds Ozoliņš, and Chris Wolverton, Particlelike Phonon Propagation Dominates Ultralow Lattice Thermal Conductivity in Crystalline Tl_3VSe_4 , *Phys. Rev. Lett.* **124**, 065901 (2020).
- [53] Yi Xia, Vinay I. Hegde, Koushik Pal, Xia Hua, Dale Gaines, Shane Patel, Jiangang He, Muratahan Aykol, and Chris Wolverton, High-Throughput Study of Lattice Thermal Conductivity in Binary Rocksalt and Zinc Blende Compounds Including Higher-Order Anharmonicity, *Phys. Rev. X* **10**, 041029 (2020).
- [54] Tao Sun and Philip B. Allen, Lattice thermal conductivity: Computations and theory of the high-temperature breakdown of the phonon-gas model, *Phys. Rev. B* **82**, 224305 (2010).
- [55] Olivier Delaire, Jie Ma, Karol Marty, Andrew F May, Michael A McGuire, Mao-Hua Du, David J Singh, A Podlesnyak, G Ehlers, MD Lumsden, *et al.*, Giant anharmonic phonon scattering in PbTe , *Nature materials* **10**, 614–619 (2011).
- [56] G. Kresse and J. Hafner, *Ab initio* molecular dynamics for liquid metals, *Phys. Rev. B* **47**, 558–561 (1993).

- [57] G. Kresse and J. Hafner, *Ab initio* molecular-dynamics simulation of the liquid-metal^{*} amorphous-semiconductor transition in germanium, *Phys. Rev. B* **49**, 14251–14269 (1994).
- [58] G. Kresse and J. Furthmüller, Efficiency of ab-initio total energy calculations for metals and semiconductors using a plane-wave basis set, *Comput. Mater. Sci.* **6**, 15–50 (1996).
- [59] G. Kresse and J. Furthmüller, Efficient iterative schemes for *ab initio* total-energy calculations using a plane-wave basis set, *Phys. Rev. B* **54**, 11169–11186 (1996).
- [60] P. E. Blöchl, Projector augmented-wave method, *Phys. Rev. B* **50**, 17953–17979 (1994).
- [61] John P. Perdew, Adrienn Ruzsinszky, Gábor I. Csonka, Oleg A. Vydrov, Gustavo E. Scuseria, Lucian A. Constantin, Xiaolan Zhou, and Kieron Burke, Restoring the Density-Gradient Expansion for Exchange in Solids and Surfaces, *Phys. Rev. Lett.* **100**, 136406 (2008).
- [62] John P. Perdew, Kieron Burke, and Yue Wang, Generalized gradient approximation for the exchange-correlation hole of a many-electron system, *Phys. Rev. B* **54**, 16533–16539 (1996).
- [63] P. Hohenberg and W. Kohn, Inhomogeneous Electron Gas, *Phys. Rev.* **136**, B864–B871 (1964).
- [64] Wu Li, Jesús Carrete, Nebil A. Katcho, and Natalio Mingo, ShengBTE: A solver of the Boltzmann transport equation for phonons, *Computer Physics Communications* **185**, 1747 – 1758 (2014).
- [65] Ion Errea, Matteo Calandra, and Francesco Mauri, Anharmonic free energies and phonon dispersions from the stochastic self-consistent harmonic approximation: Application to platinum and palladium hydrides, *Phys. Rev. B* **89**, 064302 (2014).
- [66] Terumasa Tadano and Shinji Tsuneyuki, Self-consistent phonon calculations of lattice dynamical properties in cubic SrTiO₃ with first-principles anharmonic force constants, *Phys. Rev. B* **92**, 054301 (2015).
- [67] James E. Saal, Scott Kirklin, Muratahan Aykol, Bryce Meredig, and C. Wolverton, Materials Design and Discovery with High-Throughput Density Functional Theory: The Open Quantum Materials Database (OQMD), *JOM* **65**, 1501–1509 (2013).
- [68] Scott Kirklin, James E Saal, Bryce Meredig, Alex Thompson, Jeff W Doak, Muratahan Aykol, Stephan Rühl, and Chris Wolverton, The Open Quantum Materials Database (OQMD): assessing the accuracy of DFT formation energies, *npj Computational Materials* **1**, 15010 (2015).